Journal of Structural Geology, Vol. 15, No. 11, pp. 1343 to 1357, 1993
Printed in Great Britain

0191-8141/93 $06.00+0.00

Small-scale faulting as an indicator of deformation mechanism in the Tertiary sediments of the northern Danish Central Trough

OLE RØNØ CLAUSEN and JOHN A. KORSTGÅRD

Geologisk Institut, Aarhus Universitet, DK-8000 Aarhus C, Denmark

(*Received* 6 *February* 1992; *accepted in revised form* 23 *October* 1992)

Abstract—The Tertiary sediments in the northern part of the Danish Central Trough are characterized by a large number of small faults (25–50 m offset). Models for the accommodation of the deformation of the sediments are presented and it is shown quantitatively that a bending model best explains the observed strain distribution. From this we infer that the internal deformation of the Tertiary sediments is due to differential subsidence along older fault trends and not caused by applied external stresses on the Tertiary sediments. The effect of rock rheology and excess fluid pressure is discussed in order to explain the size of the throw and the smaller number of reverse faults compared to normal faults. Although the rocks are brittle they may in regions of shortening suffer more grain-scale creep deformation than in regions of extension. The strain distribution is determined on seismic sections and the main limitations of the method is thus the vertical and horizontal resolution of the seismic surveys used.

INTRODUCTION

THE study has been carried out in the northern part of the Danish Central Trough which is part of the NNW–SSE-striking Mesozoic Central Graben located in the North Sea (Fig. 1). The mapping was concentrated on the Tertiary siliciclastic sediments which are dominated by clay interbedded with silty–sandy layers. The seismic subdivision, the ages of the sequences, and the correlation between a gamma log and the variation in grain size distribution (the variation in the clay fraction) in the Lulu-1 well is shown in Fig. 3. The sediments of the Tert1 megasequence are claystones with numerous interbedded volcanic-ash layers where Tert2 and Tert3 consists of silty claystone with numerous thin limestone layers in the oldest parts. Tert4 is dominated by a clay–claystone with frequent layers of siltstone. Tert5 is composed of a silty clay which becomes more sandy at the top (Kristoffersen & Bang 1982, Danielsen 1989).

The faulting of the Tertiary sediments is restricted to small-scale faulting (offset of less than 50 m) except around some of the major salt structures. This is in contrast to the pre-Tertiary sediments which show major faulting especially along the Coffee Soil Fault (Fig. 1) (Michelsen & Andersen 1981, Michelsen 1982, Gowers & Sæbøe 1985, Vejbæk 1986, Cartwright 1987, Vejbæk & Andersen 1987, Mikkelsen 1988, Mogensen 1988, Graversen 1989). Small-scale faulting of pre-Late Miocene rocks is also observed in the Viking Graben (Rundberg 1989), and faulting on a scale beyond the seismic resolution is observed onshore in Denmark in Middle Miocene sandy sediments (Koch & Friedrich 1970, Koch *et al.* 1973, Koch 1989).

The top Middle Miocene is the youngest surface showing significant differential subsidence along the Coffee Soil Fault trend (Clausen 1991) indicating that the pre-Late Miocene sediments are deformed due to tectonic processes. The small-scale faults in the pre-Late Miocene sediments in the North Sea reflect the present state of strain in the rocks and in this paper the distribution of strain in pre-Late Miocene sediments is used to establish a model for the deformation of the sediments.

DATA AND METHODS

Small-scale faults in the Tertiary sediments

In this study seismic lines on a 1:50,000 scale (in a few cases 1:25,000) from the surveys RTD-81, SP-82 and CGT-81 (all filtered and migrated) were used to map the Tertiary sediments (Fig. 2) (Clausen 1991). The seismic stratigraphic subdivision and the ages of the sequences are shown in Fig. 3. The top Middle Miocene located just above the Tert4 megasequence corresponds to the top of a subsequence in the Tert5 megasequence. The top of this subsequence is the youngest, faulted horizon (Clausen 1991). The subsidence across the Coffee Soil Fault during the Tertiary and thus the deformation of the Tertiary sediments is subdivided into an Early Oligocene, an Early Miocene and a Late Miocene episode (Clausen 1991).

The faults are identified from offset of identical sets of reflectors across a well defined surface. If the observed structure has a sedimentary origin, e.g. toplap, it would in most cases cause a change in the reflected waveform at each side of the 'toplap', and this is not the case for the observed structures. The offset on faults in the Tertiary sediments vary from a size beyond the seismic resolution to about 50 ms two-way time corresponding to about 50 m. The vertical resolution is less than 10–20 m at the relevant depths of the Tertiary (seismic velocity 1800–2200 m s^{-1} and frequency 40–60 Hz in the mapped interval). This means that the offset observed is well above the vertical resolution of the seismic data.

The geometry of the fault planes appears to be approximately planar, and the faults define fault blocks of 0.5–1 km width (Figs. 4 and 5). Fault block rotation

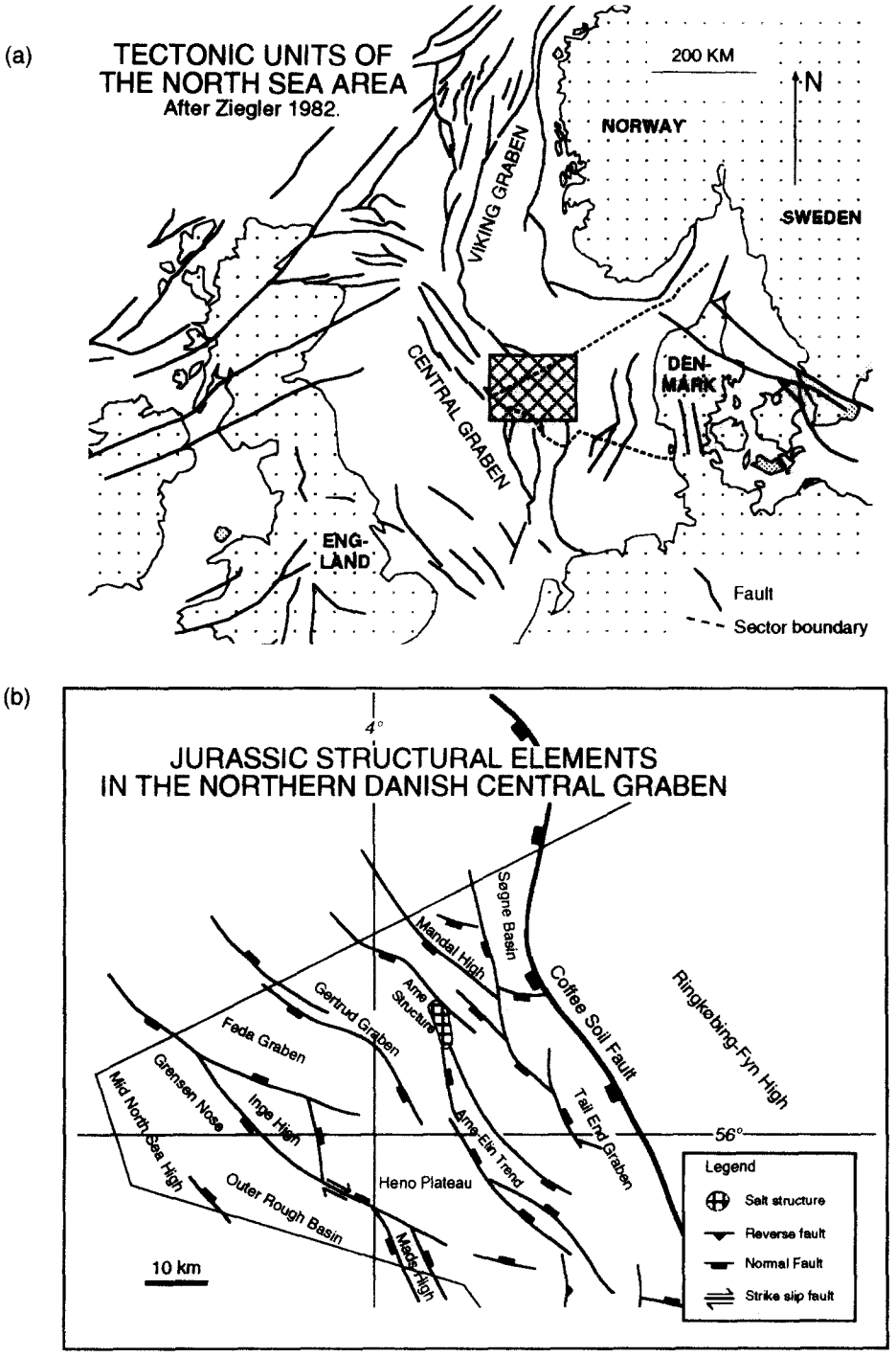

Fig. 1. (a) Structural outline of the North Sea area. The cross-hatched box indicates the location of (b). (b) The major Jurassic faults and fault blocks in the northern part of the Danish Central Trough.

may indicate that the fault planes are curved, but detachment planes cannot be observed on the seismics (Figs. 4 and 5). However, it cannot be excluded that some of the faults die out in more ductile layers which then acts as a detachment zone. The faults have not been tied from section to section, because maximum vertical offset of 50 m on the faults indicates that the total lateral length of a fault is about 3–5 km (Walsh & Watterson 1988) which means that the radius of the fault (1.5–2.5 km) is smaller than the average spacing of the seismic grid (3–7 km) (Fig. 2).

Measuring horizontal strain in a vertical section

Mapping the horizontal strain in a vertical section requires a section where faults on all scales, from cracks to major regional faults, can be observed. An approximation to an ideal vertical section is a seismic section, where the only limitation of the size of observable structures is the seismic resolution. Faults are observable when one or more reflectors are offset. Using seismic sections it is convenient to measure the bedding-parallel elongation of reflectors, since the reflectors are

assumed to represent initially horizontal, continuous strata, now faulted and therefore exhibiting bedding-parallel elongation.

Figure 6 illustrates how the elongation is calculated. A rectangular grid is superimposed on the seismic section and oriented so that the angle between the faulted reflectors and the grid axis is, on average, minimized. The grid spacing is chosen so that there is usually only one fault within each grid cell. The measured length of a reflector within a grid cell, for example $a + b$ in Fig. 6, then represents the original length and the post-faulting or present length is represented by the grid spacing. The horizontal resolution, which is determined by the radius of the first fresnel zone, is thus of great importance since it will influence the determination of the location of the fault plane cut-off of the beds. In practice it means that the bed termination on each side of a normal fault will appear to be closer than they really are (i.e. the measured elongation will be smaller than the 'true' elongation) or even overlap, which may obscure the orientation of the fault plane. However, this will only affect the absolute size of the elongation because the dip of the fault plane (and thus the sense of the fault) is unaffected by the horizontal resolution because the radius of the first Fresnel zone is equal for different beds cut by the same fault, when dealing with small-scale faults. The length of the faulted bed is therefore measured after determination of the fault plane and the effect of the horizontal resolution is minimized. The determination of the fault plane also gives an impression of the angle between the vertical section and the fault plane because a dip of approximately 40–60° is expected and observed at crossing seismic sections. Faults with an unrealistic low dip and large heave will therefore be ignored.

Following this procedure each grid cell is assigned an elongation value. Elongation values are positive when faulting is normal and negative when faulting is reverse ($c + d$ in Fig. 6). The elongation values are contoured, and the contour pattern shows the distribution of strata parallel elongation in the vertical section. It should be noted that the contours only show the variation of elongation in that particular vertical section and not the variation in size or orientation of the principal axes of strain.

Horizontal strain in vertical sections across the Coffee Soil Fault

In the Danish Central Trough area there is a concentration of faults in sequences above major gradients on the Top Chalk surface. Reflector-parallel elongation in these sequences has been mapped along six seismic lines crossing the Coffee Soil Fault at high angles (Fig. 7).

In the Tertiary sequences Tert1 and in part Tert3 (Early Oligocene) little or no faulting is observed. The lack of recorded deformation in Tert3 is probably due to poor reflectivity. Minor disturbances of the continuous reflectors at the top of Tert3 are interpreted as faults, and since it is possible to identify faults in the parts of the Tert3 sequence where reflectivity is good, it thus appears that the Tert3 sediments were deformed in a brittle manner.

The Tert1 sequence (Late Paleocene and Early Eocene) is dominated by clay (Kristoffersen & Bang 1982, Nielsen *et al.* 1986, Danielsen 1989), and is an excellent sealing rock above faulted chalk reservoirs at several oil fields in the North Sea. The parallelism between the Interval Time maps (in two-way time) of the Top Chalk and the Top Tert1 (Clausen 1991) indicates that the Tert1 sediments have suffered approxi-

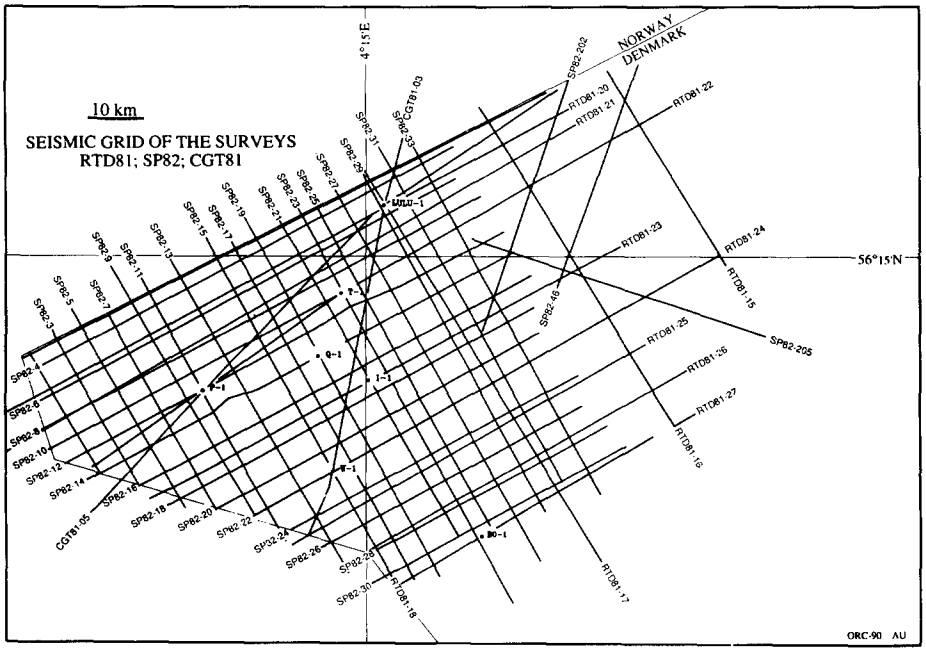

Fig. 2. The seismic grid used for mapping the Tertiary siliciclastic sediments. The grid spacing precludes the lateral tie of small-scale faults.

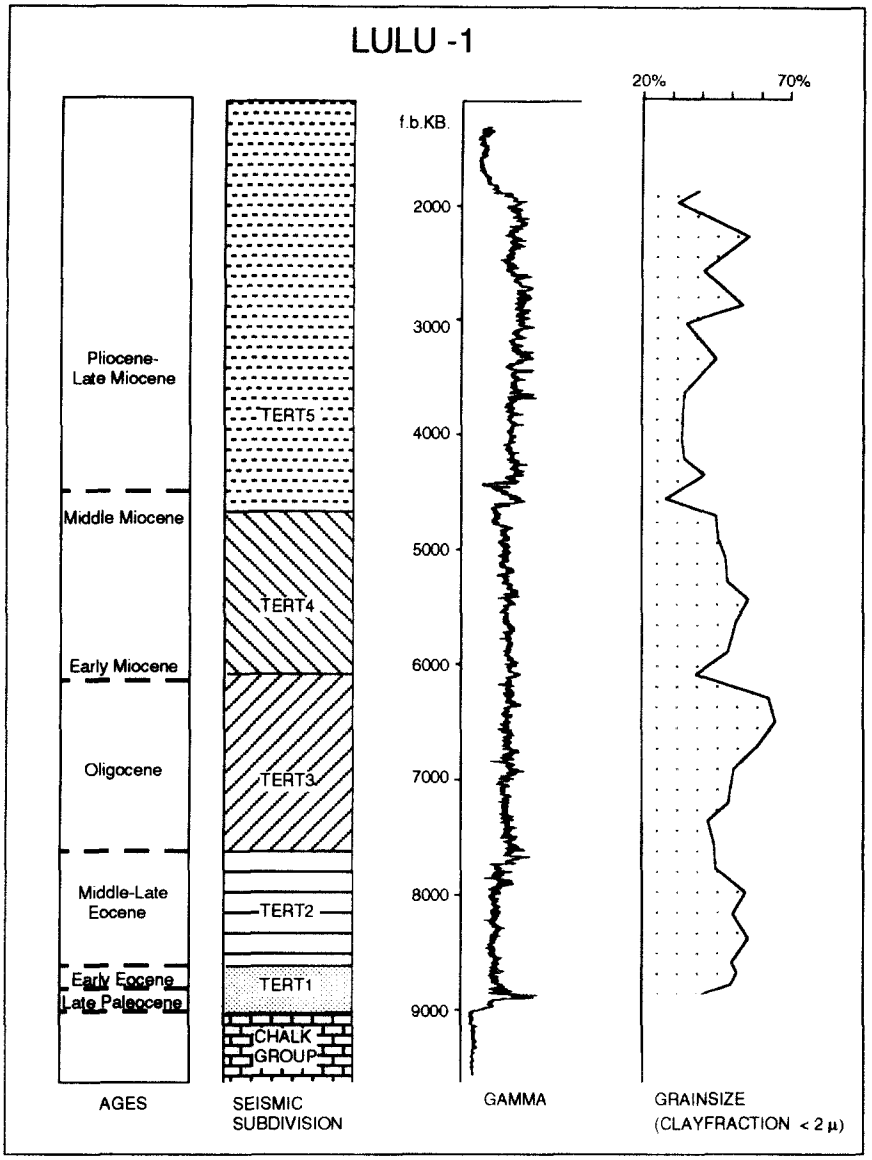

Fig. 3. Correlation between seismic stratigraphic subdivision, age, gamma ray log and the percentage of clay-size particles in the sediments. The seismic stratigraphic subdivision and dating is from Clausen (1991), and the lithological informations from Danielsen (1989).

mately the same amount of deformation as the Top Chalk surface. The lack of observed faults in the Tert1 sediments is therefore probably because the clay-dominated sediments responded in a ductile manner to the imposed deformation and because of a lower limit of seismic resolution due to an increasing seismic velocity.

In general elongation is positive (normal faulting) along the sections (Fig. 7). However, negative elongation (reverse faulting) is seen in several sections and mainly above the Coffee Soil Fault. The contour pattern of the parallel elongation partly reflects the shape of the deformed sequences and there is a lateral change from positive to negative elongation within each sequence. There is also a tendency in some sections for the contours to parallel the sequence boundaries (e.g. RTD81-20 and RTD81-25), while other sections show isolated islands of positive and negative elongation due to the dying out of series of faults. The lack of elongation data from the Tert3 sequence also enhances the visual perception of parallelism.

DEFORMATION MODELS

For the origin of the small-scale faults in the Tertiary sediments of the northern Danish Central Trough, a pure shear strain or bending model is favoured and described first. Gravity and simple shear strain models are discussed briefly later.

The Top Chalk surface indicates the total differential subsidence during the Tertiary and since the lowermost Tertiary sediments (Tert1) are dominated by clay both in grain size and mineralogically (Nielsen *et al.* 1986, Danielsen 1989) all models assume a detaching layer between the Tertiary siliciclastics and the Chalk Group

in the Tert1 sediments which have a very low shearing resistance.

Pure shear strain or bending model

The bending will be regarded as a two-dimensional plane strain. The bending model assumes that the sedimentary layer is bent around an axis and that there is a horizon or surface (a line in two dimensions) of no deformation (Ramsay 1967, p. 401). In the deformed state an initially horizontal layer can be subdivided into several segments each with a different curvature (Fig. 8) and therefore different bending axes.

As shown quantitatively in Appendix 1, the parallel elongation depends on the location of the strata with respect to the surface of no deformation and the curvature of the layer. Within each segment the parallel elongation is therefore constant along concentric circles centered at the bending axis (Appendix 1, Fig. A1). Due to the change from an upward concave to an upward convex configuration along the deformed strata it is possible for both compression and extension structures to occur in the same layer during the same bending event (Fig. 9a).

It is possible to test the application of the bending model to the northern part of the Danish Central Trough in a semi-quantitative way. Seismic stratigraphy gives the ages of sequence boundaries that are taken to be horizontal and planar at the time of deposition (or generation if an erosional surface). The present shape of a sequence boundary therefore reflects the accumulated strain of all the deformations applied to the sediments below the sequence boundary after the generation of the sequence boundary. The accumulated deformation can be divided into separate episodes by performing a forward calculation on depth converted sections. Consider an initially horizontal surface, 'Top A' (Fig. 10). After the next sequence B is deposited the top A surface has a lateral shape reflecting the deformation introduced to the sediments below the top A surface during the deposition of sequence B. The procedure is repeated when introducing the next sequence C, whose top is horizontal at the time of deposition. The shape of the top of sequence B now reflects the deformation introduced to the sediments below top B, i.e. the deformation of the B sequence and also the additional deformation to the previously deformed A sequence (Fig. 10).

In the forward calculations performed here the neutral surface is placed at the top of the sequence that indicates the deformation of the episode in question, and the deformation is assumed to be plane strain. The location of the neutral surface is critical and if it was located at the base of the Tertiary sediments the deformation pattern would be like the upper part of the layer in Fig. 9(a), i.e. very different from the oberved pattern. The only way to achieve a calculated strain pattern like the observed is when the neutral surface is located in the upper parts of the sequence and for convenience during the calculations it is located at the top of the sequence.

The forward calculations have been performed on the section RTD81-22 by choosing a number of sequence boundaries (top Tert2, top Tert3, top Tert4.3, top Tert4) that can be assumed to have been horizontal when they were deposited (Clausen 1991). The shape of

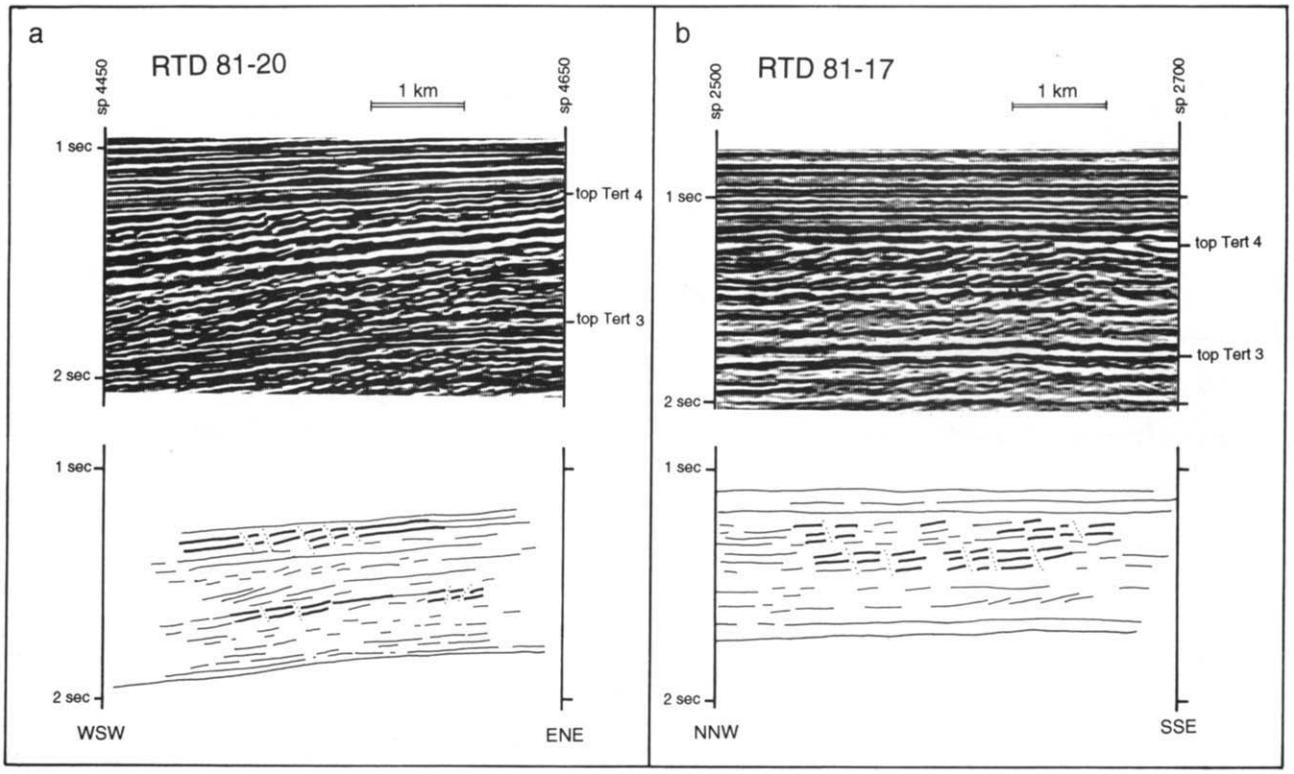

Fig. 4. Examples of the small-scale faults illustrated by seismic sections and line drawings. (a) and (b) show normal faults in sections oriented WSW–ENE and NNW–SSE, respectively. There are a few reverse faults in (a).

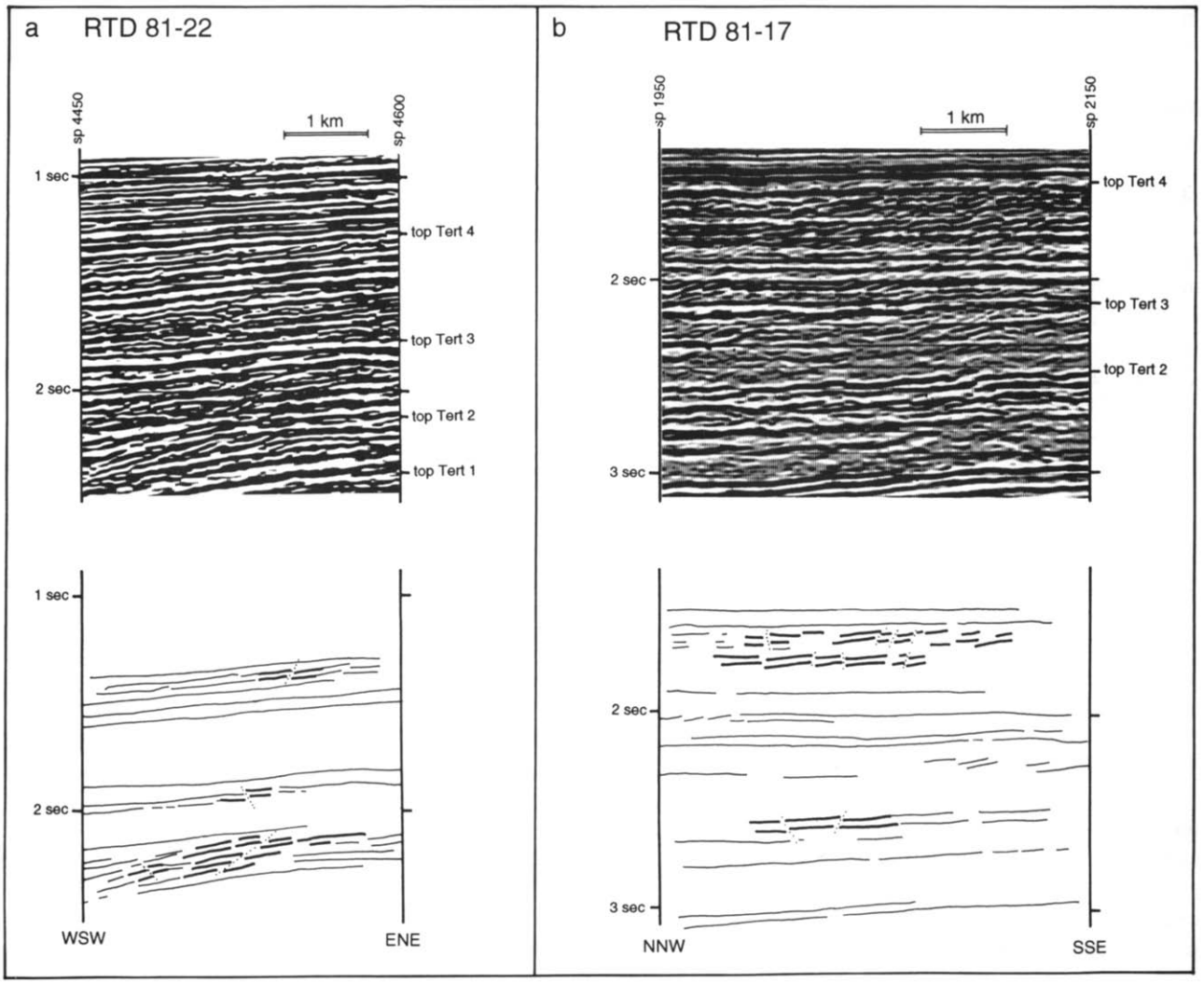

Fig. 5. (a) and (b) show reverse and normal faults in sections oriented WSW–ENE and NNW–SSE, respectively. The line drawings do not show all faults present in the sections.

a sequence boundary in a backstripped section is used to calculate the horizontal elongation introduced to the sediments below the sequence boundary. The total horizontal elongation is determined by accumulating the elongation introduced during each period as outlined above. The calculations are described in detail in Appendix 1. The accumulated horizontal elongation at a number of points is contoured to test the bending model by comparing the calculated contour pattern to the measured contour pattern. The calculations are performed on a depth converted section to get the best approximation of the angle between the two limbs of the bended surface. It is only possible to change the shape of the surface from convex upwards on the time section to convex downwards on the depth section if the stack velocity gets significantly lower from the east to the west (i.e. down-dip of the surface). The interval and stacking velocities vary systematically in the area and gets higher to the west (Nielsen & Japsen 1991) as expected because the sediments there are buried deeper. This means that velocity variations in the depth conversion may change the absolute value but not the sign of the calculated elongation.

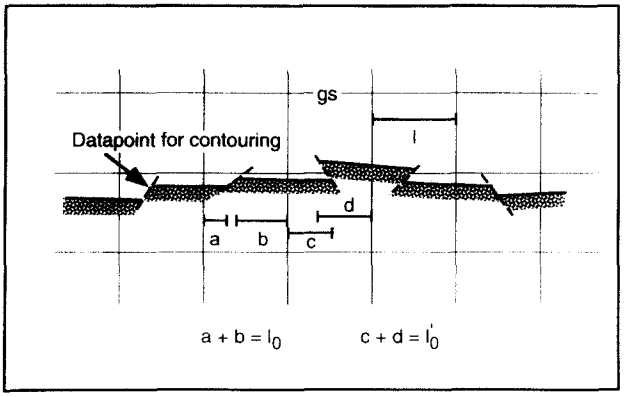

Fig. 6. The principles of measuring the horizontal elongation. The grid is oriented approximately parallel to the present orientation of the beds on which the elongation is measured. The grid spacing (gs) is chosen so that each grid cell on average contains one fault. The lengths a and b (or c and d) added give the original length of the bed (l_0) whereas the present length of the bed is represented by the grid spacings (gs).

A comparison of the measured and calculated parallel elongation shows qualitative match between the major compressional and extensional areas (Fig. 11). The most evident differences are observed in the sequences where there are no observed elongations due to poor seismic resolution, e.g. the calculated compressional strain

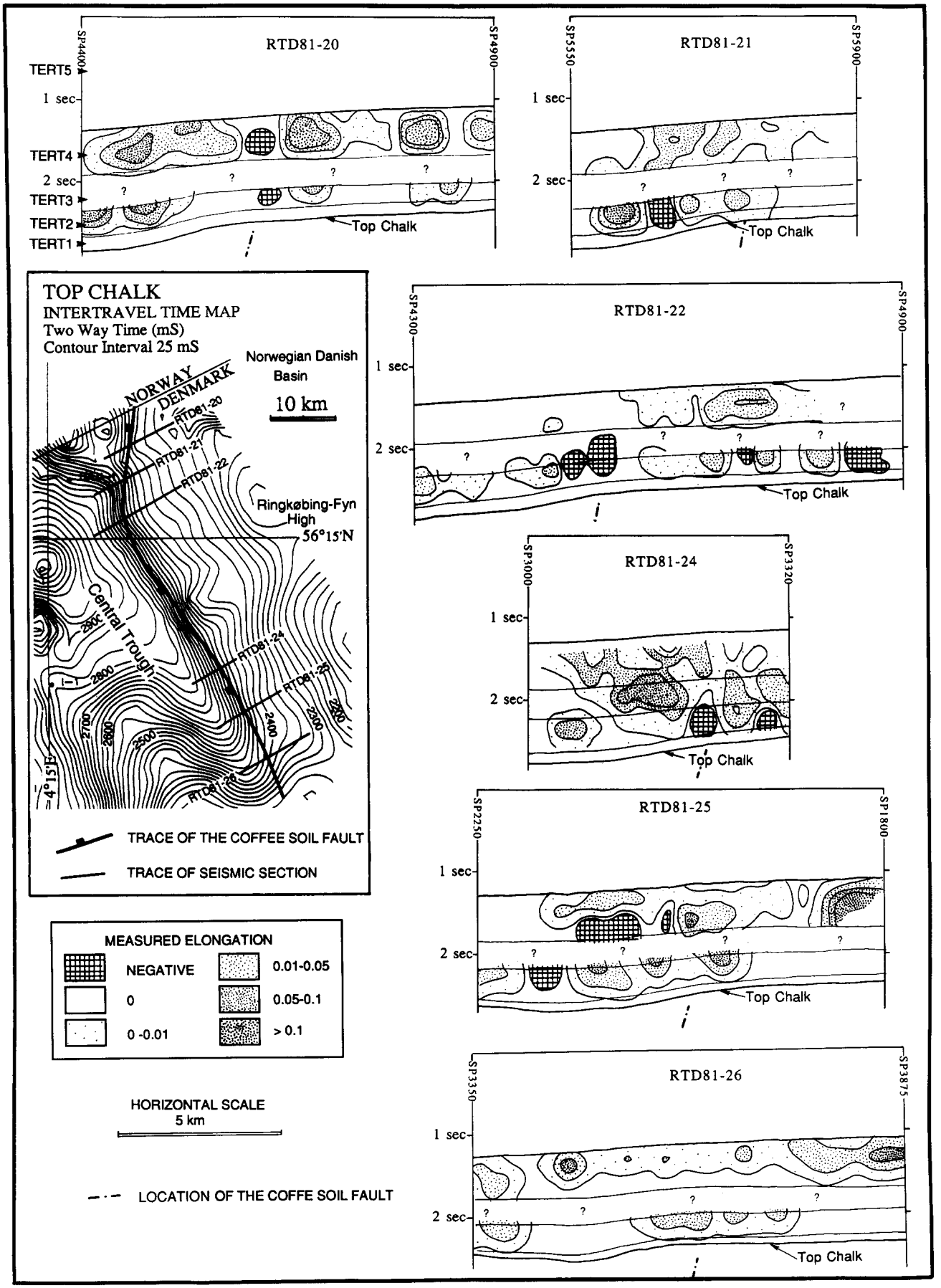

Fig. 7. The Top Chalk surface shows the total differential subsidence since deposition of the Danian Chalk. The Coffee Soil Fault, which is the eastern limitation of the Central Graben, does not penetrate the Chalk units. However it is shown here to illustrate the juxtaposition of the major gradient on the Top Chalk surface and the fault. The locations of the seismic sections, which are the basis for the measuring of the horizontal elongation is also indicated. The cross-sections are based on the seismic sections and the elongation ε is calculated and contoured using the indicated contour intervals. The horizontal scale of the sections does not correspond to the horizontal scale of the map. The cross-sections show a vertical subdivision (indicated by thin lines) which corresponds to the seismic sequences of Figs. 4 and 5. However the top Tert5 boundary is excluded since the small-scale faults are absent in the Tert5 sequence.

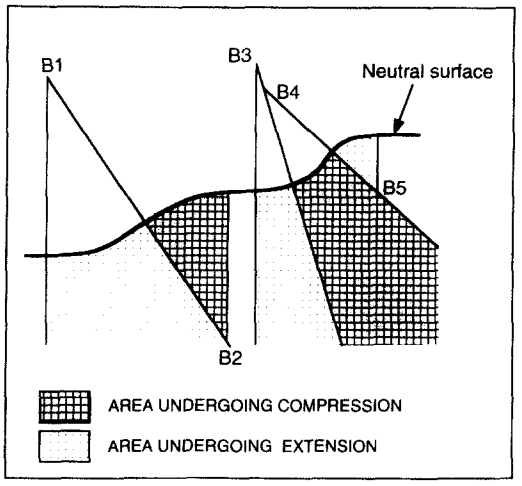

Fig. 8. The principle of subdividing the shape of a horizon into segments which suffer compression or extension depending on the distance to the bending axes (B1–B5).

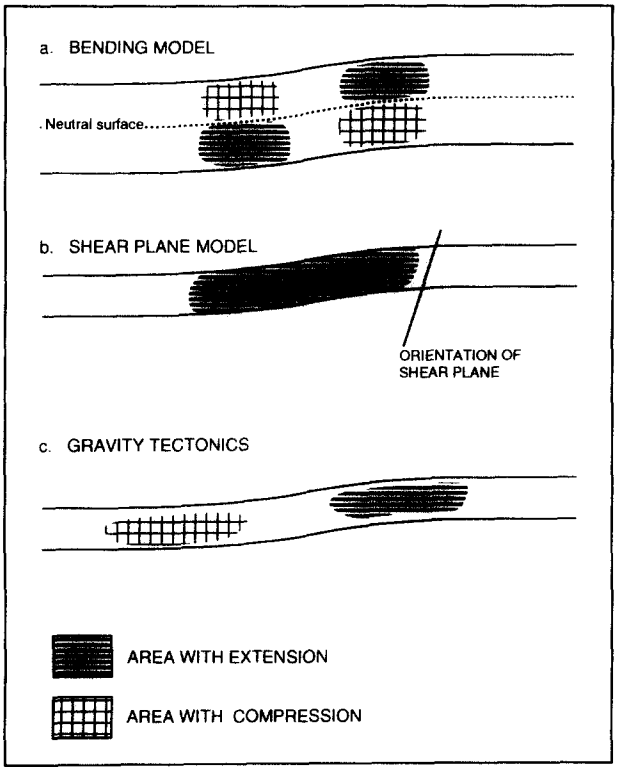

Fig. 9. The strain distribution in a vertical section is the response of a layer to deformation caused by the differential subsidence of the 'basement'. The ideal strain distribution resulting from (a) a bending model, (b) a shear plane model and (c) gravity tectonics is illustrated. The strain distribution of the shear plane model depends on the orientation of the shear plane with respect to the shear direction, and only a shear plane with a dip in the opposite direction and with the shown differential subsidence would result in compression instead of extension.

within the lowermost sequence (Tert1) in the eastern part of the sections of Fig. 11. The compression might nevertheless be present since a core from this sequence in the T-1 well (Fig. 2) shows shearing, indicating that the Tert1 sediments at T-1 are intensely deformed on a scale below the seismic resolution. The similarity of the areas of compression above the major gradient on the

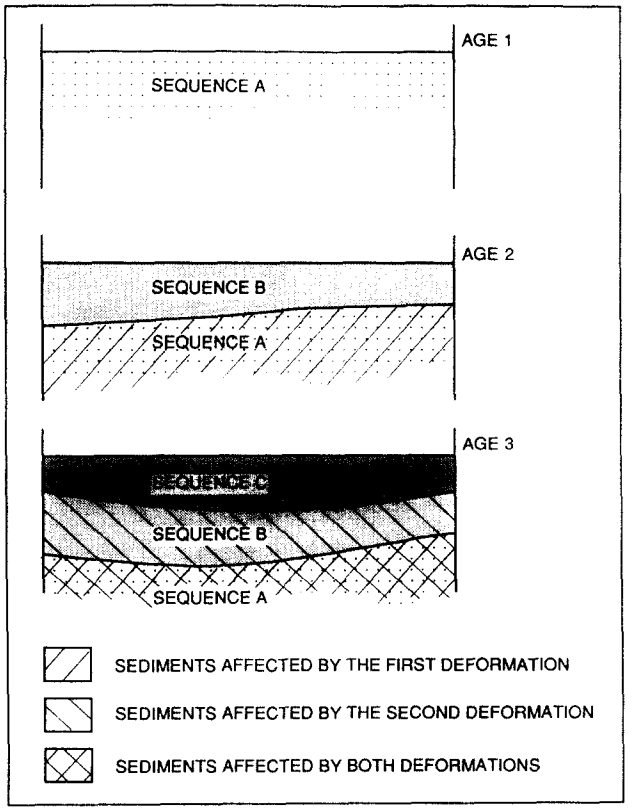

Fig. 10. Diagram illustrating how the surface of a sequence indicates the accumulated strain (deformation) that the sequence has suffered due to differential subsidence. At age 1 the sequence A is deposited and the top of A is assumed planar and horizontal. At age 2 the sequence B is deposited and the top of B is assumed planar and horizontal. The top of A now shows how the sequence A is affected by the first deformation. At age 3 the sequence C is deposited and the top of C is assumed planar and horizontal. The top of B shows the deformation, which affects the sediments of sequence B and sequence A. Sequence A is thus deformed twice, which is reflected in the top of A. This is the principle used in the forward calculations for the simple modelling of the strain distribution.

Top Chalk and the major extension in the basin to the west is convincing (Fig. 11). The patchy contour pattern of the measured elongation in the lowermost east-northeast part of the measured section (Fig. 11a) is somewhat different from the calculated section. The reason for this may be the way the forward calculations are performed, since an area that has undergone compression followed by extension may end up having a net extension which in the calculations will show up as a positive elongation. However, the patchy contour pattern in some measured sections may also indicate that subsequent extension did not eliminate any previous compression but was distributed along another set of faults, i.e. there was only a limited reactivation of faults. The simple calculations of the model do not take reactivation of previously generated faults with opposite sense of displacement into account. The influence of the rheological properties of the sediments controlling the generation of faults is also neglected.

Simple shear strain model

In a model where the differential subsidence is accommodated by a simple shear strain, the horizontal

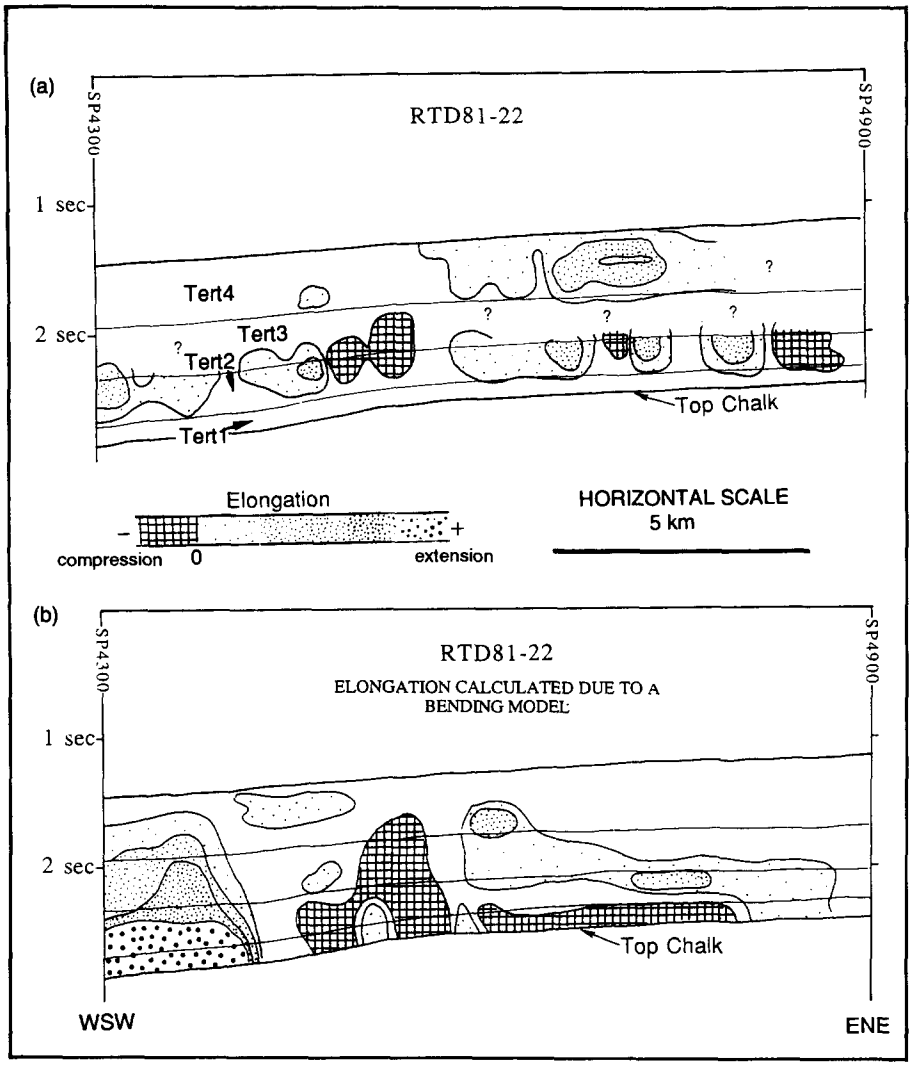

Fig. 11. Cross-sections showing the distribution of (a) the measured and (b) the calculated horizontal elongation from the seismic section RTD81-22 (for geographical location see Fig. 7). The calculations are performed on depth converted sections, and the result is to facilitate the comparison with the observations transformed into a time section. See text for discussion of similarities.

elongation at a given location is controlled by the dip of the deformed layer before and after deformation, the dip of the shear plane, and the amount of simple shear strain. The mathematics are given in Appendix 2. Due to the nature of simple shear, the horizontal elongation value is constant in a plane that parallels the shear plane. A generalized distribution of horizontal elongation when using a simple shear model is shown in Fig. 9(b). A differential subsidence across a zone of simple shear can only give a negative elongation (compression) if the angle between the subsiding part of the deformed strata and the displacement vector exceeds 90°.

The simple shear model can hardly account for the observed deformation structures in the Tertiary sediments of the northern part of the Danish Central Trough, since it is only possible to get positive and negative elongation along the same strata if the sense of displacement along the shear plane or the orientation of the shear plane changes. Thus a simple shear model would require a complicated and speculative array of shear planes and shear directions to account for the observed strain distribution.

Gravity tectonics

There are other deformation mechanisms than bending that may generate small-scale faults similar to the ones observed. Gravity tectonics relevant to the Tertiary siliciclastic rocks are gravity gliding and gravity spreading (Ramberg 1981). Although gravity gliding and gravity spreading differ in the way internal mass transport takes place (Galloway 1987, Schack Pedersen 1987), both mechanisms are characterized by compressional structures at the base of the slope and extensional structures at the top of the slope (Dailly 1976, Winker 1982) (Fig. 9c). This strain pattern is also characteristic of gravity tectonics at prograding shelf margins (Galloway 1987). However, gravity tectonics cannot account for the deformation observed in the Tertiary sediments of the northern part of the Danish Central Trough since the measured sections show an upslope location of the negative elongation where the gravity model requires a downslope location. Series of slides on a scale smaller than the entire slope would give a strain contour pattern alternating between positive and negative elongation

parallel to the strata and this is not observed on the mapped sections.

DISCUSSION OF METHODS AND MODELS

Influence of the orientation of the seismic section on the measured horizontal elongation

A strain ellipsoid with the principal axes X, Y and Z can be defined for any point of the deformed strata. At any location, where stretching or compression in a horizontal direction has taken place, the intermediate axis Y is horizontal and normal to a vertical XZ-plane, with X and Z horizontal or vertical. If the horizontal elongation is measured in an arbitrary direction with respect to the principal axes of strain the measured elongation (ε_m) will depend on the amount of stretching (or compression) and on the angle, v, between the direction in which the elongation is measured and the vertical XZ-plane in the horizontal plane (Fig. 12).

The apparent quadratic elongation

$$\lambda_m = (1 + \varepsilon_m)^2 \quad (1)$$

is a function of v and the true quadratic elongation λ_t

$$\lambda_m = \lambda_t \cos^2 v - \sin^2 v. \quad (2)$$

The normalized deviation

$$d = \frac{\lambda_t - \lambda_m}{\lambda_t} \quad (3)$$

indicates that d is a function of v due to equation (2). Figure 13 shows the variations of the normalized deviation with respect to v. The non-symmetry around zero in Fig. 13 shows that the absolute normalized deviation is larger for a given negative elongation than for a corresponding positive elongation. Therefore, to compare the absolute value of compression and extension from a measured elongation the angle v must be known. However, assuming that the elongation in the Y-direction is zero (plane strain), as is done in Fig. 13 and when dealing with passive deformation due to differential subsidence, the sign of the elongation does not change with a change in v. Therefore parts of a section where a horizontal compression is measured have also suffered horizontal compression.

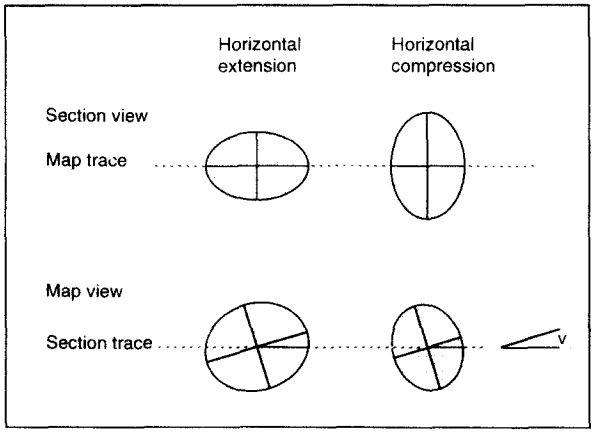

Fig. 12. Section and map view of the strain ellipsoid. The measured elongation in the section view must be corrected depending on the value of v in map view.

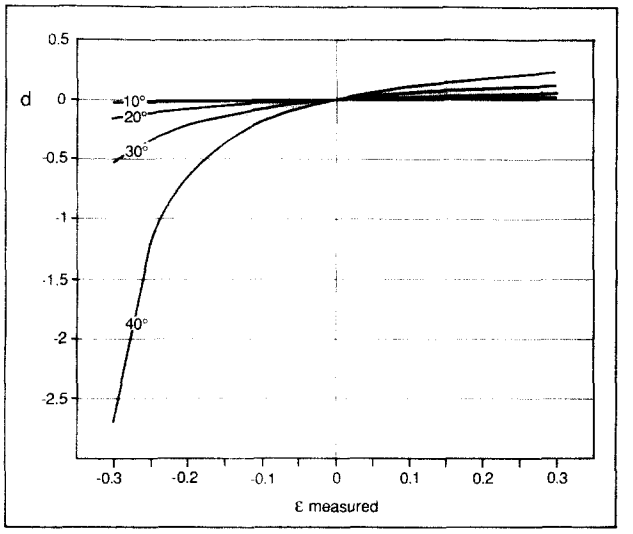

Fig. 13. Graph showing d (see text, equation 3) as a function of the measured elongation (ε measured) and the angle v (Fig. 12) between the principal strain axis X or Z and the seismic section.

Sub-seismic deformation

Bulk deformation accommodated along faults with a throw smaller than the seismic resolution cannot be observed in seismic sections. In the Tertiary rocks in the northern Danish Central Trough the lower limit of the seismic resolution is about 10–20 m. A fraction of the total deformation is not measured when only fault displacements from seismic sections are considered because the number of faults (structurally introduced displacements) increases with decreasing displacement along the individual faults–fractures, i.e. the measured elongation is smaller than the true elongation (Childs *et al.* 1990, Marrett & Allmendinger 1991, Walsh *et al.* 1991). However, the spatial clustering of sub-seismic faults and faults observable on seismic sections infers that the sub-seismic faults will have no effect on the distribution of strain (Gauthier *et al.* 1991). The deformation accommodated by structures of a size below the seismic resolution passes as ductile deformation (Groshong 1988) on a seismic scale, because the deformation appears to be homogeneously distributed and there is no visible rupture. This emphasizes the scale dependence of recognizing brittle vs ductile deformation.

Influence of the state of stress on the generation of reverse faults vs normal faults in a bending model

The primary response of a layer suffering deformation is elastic deformation with the consequent build-up of differential stress. The stress build-up relaxes by faulting and/or by flow (ductile deformation) and the elastic strain is transformed into a permanent strain. The faults

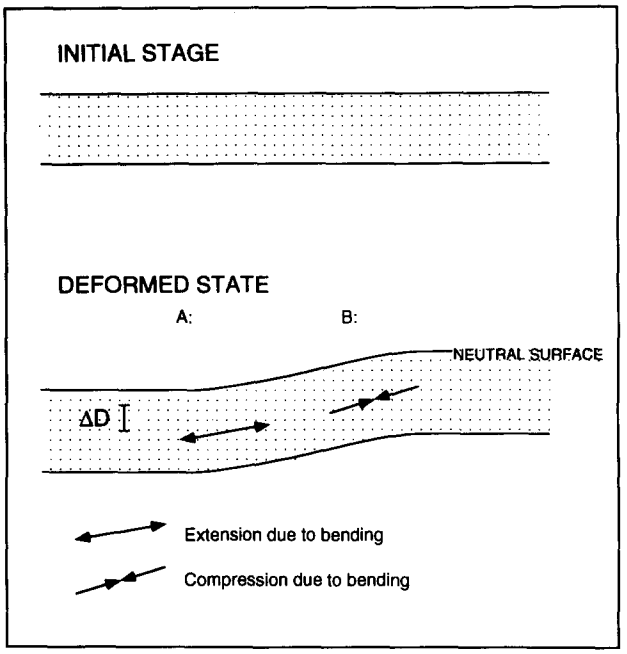

Fig. 14. Orientation and location of the stress generated due to bending of an initially planar bed under differential subsidence. The difference in depth between location A and location B is ΔD.

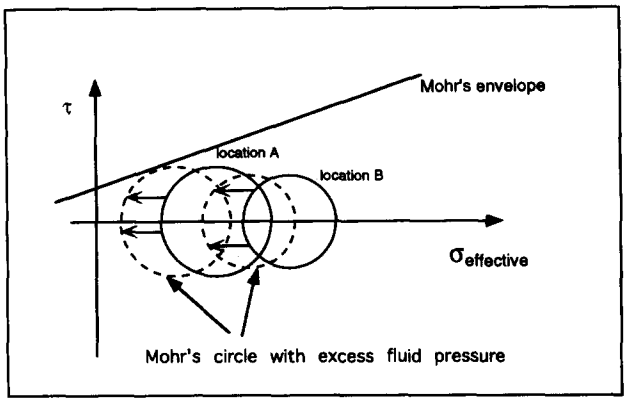

Fig. 15. Mohr circles representing the state of stress at locations A and B of Fig. 13 with respect to a linear Mohr envelope and assuming the same amount of bending at A and B. The size and position of the Mohr circles shows that faulting at location A will initiate at a smaller bending than at location B. The effect of excess fluid pressure will reduce the strength of the rock, which is reflected in the relative leftward shift of the Mohr circles with respect to the Mohr's envelope.

in the Tertiary sediments reflect the relaxation of the local build-up of differential stress due to bending and not due to imposed external stresses.

Figure 14 outlines a simple model of the Tertiary subsidence of the Danish Central Trough where the faults at location B below the neutral surface are dominantly reverse faults (horizontal compression) and normal faults at location A (horizontal extension). A common observation in the northern Danish Central Trough is that the number of reverse faults at location B is smaller than the number of normal faults at location A, even though the strain is comparable at A and B. However, the displacement along the reverse faults seems to be larger than the displacement along the normal faults.

A stress–strain analysis of the simple model may reveal the reasons for the differences in fault distribution at location A and location B. The bending of a bed as indicated in Fig. 14 introduces differential stress due to strain–stress relations since the principal axes of strain will be parallel and perpendicular to the bent surface (Hobbs 1971). Having the compressive stresses as positive and assuming that the bending at location A in Fig. 14 is comparable to the bending at location B (i.e. the curvature is the same and the neutral surface is located at the top of the stratum), it is shown that the differential stresses at A are larger than at B and that the least compressive stress at A is smaller than at B (Appendix 3) for the materials and depths present in the study area.

The relative location of the Mohr circles (Fig. 15) thus shows that faulting will initiate at a lower differential stress at A than at location B (Fig. 14), corresponding to a smaller amount of bending. The differential stress generated during bending is relaxed around a fault where the elastic deformation is transformed into a permanent deformation. The areas adjacent to the first initiated fault still support a certain amount of differential stress due to bending and further bending may initiate a population of genetically related faults. The higher differential stress required to initiate faults at location B implies that a fault, when generated at B, has a larger displacement due to the larger elastic strain stored before faulting and released during faulting at location B than at location A. The normal faults are thus more numerous than the reverse faults but the displacement along the normal faults is smaller since the total strain which is accommodated at location A and location B is comparable.

If we assume identical evolution of bending at locations A and B then the rocks at location B are stressed by a larger differential stress without faulting during a longer period than the rocks at location A. This means that there will be a larger fraction of the elastic deformation transformed into permanent deformation by creep at location B than at location A. The plastic deformation at B results in less deformation to be accommodated by faulting at location B than at location A, which again contributes to the unequal distribution of fault types.

The effect of depth conversion

It is necessary to depth convert the seismic time sections in order to obtain the true angle between the two flanks of a bent surface to give the best approximation to the bending induced strain. Critical to the depth conversion are the seismic velocities chosen. However, it is only possible to change the shape of a convex upwards surface to a convex downwards (or vice versa) if the interval velocity laterally gets dramatically lower down-dip on Fig. 14. In the eastern part of the Danish Central Trough the interval velocity down-dip increases due to the deeper burial of the sediments (Nielsen & Japsen 1991). This means that the influence of the depth conversion is to get a better approximation

of the true angle between the flanks. Minor errors in the velocities are not critical to the sign of the calculated elongation, only to the absolute value.

The effect of compaction

In the bending model the shape of an initially horizontal marker horizon (in this case a sequence boundary) is assumed to indicate the deformation of the sediments below the horizon (Fig. 10). The subsidence of a horizon may be subdivided into basement subsidence and subsidence due to compaction of the sediments between the basement and the horizon. In this case the Top Chalk is taken as basement, since it shows the total differential subsidence during the Tertiary. The compaction of the pre-Tertiary sediments is thus included in the basement subsidence. The horizontal strain in a sequence may therefore arise from basement subsidence, compaction of the sediments below the sequence and compaction of the sequence itself.

The differential compaction of the sequence itself introduces a positive horizontal elongation since differential compaction may be compared to a simple shear model with a vertical shear plane. This means that the elongation is positive and fairly constant across the zone of differential subsidence.

The general pattern during the Tertiary is differential subsidence of the basement (Top Chalk) across the Coffee Soil Fault. This is reflected in the depositional pattern with thicker sediments in the Tail End Graben than on the Ringkøbing–Fyn High. The compaction effect on the subsidence of a horizon will therefore reflect the pattern of true basement subsidence. If the compaction subsidence is accommodated by bending of individual layers, the horizontal strain distribution will be the same as if all the subsidence is basement subsidence when calculating the horizontal elongation, especially with respect to the location of compression and extension. The compaction is thus neglected during the backstripping and calculation of horizontal strain. However, if the deformation of a sequence is induced by compaction of the sediments below the sequence, and the sequence is deformed by bending, there is a need for a detachment similar to the detachment at the basement–sediment boundary as outlined in the deformation models. The calculated strain in Fig. 11(b) in the lowermost sequences indicates that there is a detachment at a level within the Tertiary sediments since the calculated compressions are too large and not observed on the seismic sections.

The influence of the excess fluid pressure to fault generation

The hydrostatic pressure is of importance to the generation of faults because the pore pressure influences the strength of the rock. An excess fluid pressure will weaken the rock and a fluid pressure less than the hydrostatic pressure will strengthen the rock (Scholz 1990, pp. 30–31). Excess fluid pressure will move the Mohr circles to the left in an effective normal stress vs shear stress diagram (Fig. 15) and the differential stress required to initiate faulting is therefore smaller when excess fluid pressure is present. This means that faulting initiates at a smaller elastic strain during progressive bending.

There are several indications of excess fluid pressure in the Tertiary rocks of the northern Danish Central Trough at present (Kristoffersen & Bang 1982) and it is interesting to note that the shallowest depth of the 'overpressured shales' corresponds to the top of the intensely faulted Tert4 seismic unit (Kristoffersen & Bang 1982). However, detailed modelling, which is beyond the scope of this paper, would be required to provide estimates of the spatial and temporal evolution of overpressuring and create a link between the observed tectonics and the state of pressure.

CONCLUSIONS

The strain distribution in the Tertiary sediments in the Danish Central Trough can be explained by a simple bending model where the Tertiary siliciclastic sediments constitute a layer decoupled from underlying chalk. The bending of the Tertiary sediments is caused by differential subsidence of the pre-Tertiary rocks, and the deformation is accommodated mainly by slip on minor faults. The generation of faults is enhanced by the presence of excess fluid pressure. There are indications that the Tertiary sediments may be subdivided into several detached units.

The larger number of normal faults relative to the number of reverse faults and the smaller displacement at each individual normal fault compared to the displacement along reverse faults is caused by the relative size and orientation of the stresses generated due to the stress–strain relations of elastic deformation which precedes faulting. The differential stress is generated by bending, and using the applied simple bending model it is shown that the differential stress required to generate normal faults is smaller than the differential stress required to generate reverse faults. The elastic deformation stored in areas with compression is thus larger and persists longer than in areas with extension before faulting transforms the elastic strain into a permanent strain. A consequence of the latter is that 'slow' creep processes may work and transform the elastic strain into a permanent strain without faulting.

When observing deformed rocks on seismic sections it is important to be aware of the limit of seismic resolution and the fault displacement density of the strata in question before classifying the deformation as ductile or brittle since this classification is scale dependent. The term 'seismo-ductile deformation' may be used for deformation accommodated by brittle deformation structures on a scale smaller than can be observed on seismic sections.

Acknowledgements—Ole Rønø Clausen acknowledges receipt of a grant from the Science Faculty, Aarhus University. We would like to

thank John Walsh and Ian Lerche for comments on earlier versions of the manuscripts and our reviewers, R. W. Allmendinger and M. A. Naylor, for very constructive criticism.

REFERENCES

Birch, F. 1966. Compressibility; elastic constants. In: *Handbook of Physical Constants* (edited by Clark, S. P.). *Mem. geol. Soc. Am.* **97**, 97–175.

Cartwright, J. 1987. Transverse structural zones in continental rifts—an example from the Danish sector of the North Sea. In: *Petroleum Geology of North West Europe* (edited by Brooks, J. & Glennie, K. W.). Graham & Trotman, London, 441–453.

Childs, C., Walsh, J. J. & Watterson, J. 1990. A method for estimation of the density of fault displacements below the limits of seismic resolution in reservoir formation. In: *North Sea Oil and Gas Reservoirs, II* (edited by Buller *et al.*). Graham & Trotman, London, 309–318.

Clausen, O. R. 1991. Tertiary seismic, stratigraphic and structural evolution of the northern Danish Central Trough. Unpublished Ph.D. thesis, Aarhus University. Denmark.

Dailly, G. C. 1976. A possible mechanism relating progradation, growth faulting, clay diapirism and overthrusting in a regressive sequence of sediments. *Bull. Can. Petrol. Geol.* **24**, 92–116.

Danielsen, M. 1989. En sedimentologisk undersøgelse af Tertiære sedimenter i de danske Nordsøboringer Lulu-1 og Inez-1. Unpublished Masters thesis, Aarhus University, Denmark.

Galloway, W. E. 1987. Depositional and structural architecture of prograding clastic continental margins: tectonic influence of patterns of basin filling. *Norsk geol. Tidsskr.* **67**, 237–253.

Gauthier, B. D. M., Lake, S. & Jensen, Y. 1991. Probablistic Modeling of Subseismic Faults in the Pelican Field (Block 211/26a), North Sea, Offshore U.K. *Bull. Am. Ass. Petrol. Geol.* **75**, 579.

Gowers, M. B. & Sæbøe, A., 1985. On the structural evolution of the Central Trough in the Norwegian and Danish sectors of the North Sea. *Mar. & Petrol. Geol.* **2**, 298–318.

Graversen, O. 1989. Basin analysis of the Danish Central Graben. CENBAS Project A: structural analysis. Internal CENBAS report, Copenhagen University, Denmark.

Groshong, R. H. 1988. Low-temperature deformation mechanisms and their interpretation. *Bull. geol. Soc. Am.* **100**, 1329–1360.

Hobbs, B. E. 1971. The analysis of strain in a folded layer. *Tectonophysics* **11**, 329–375.

Hobbs, B. E., Means, W. D. & Williams, P. F. 1976. *An Outline of Structural Geology*. John Wiley & Sons, New York.

Jaeger, J. C. & Cook, N. G. W. 1969. *Fundamentals of Rock Mechanics*. John Wiley & Sons Inc.

Koch, B. E. 1989. Geology of the Søby–Fasterholt area. *Danmarks geol. Unders.* **A22**.

Koch, B. E. & Friedrich, W. 1970. Geologisch-Palaobotanische Untersuchung der Miozänen Braunkohlen bei Fasterholt in Jutland, Dänemark. *Bull. geol. Soc. Denmark* **20**, 169–191.

Koch, B. E., Friedrich, W., Christensen, E. F. & Friis, E. M. 1973. Den Miocæne brunkulsflora og dens geologiske miljø i Søby-Fasterholt området sydøst for Herning. *Dansk geol. Foren. Årsskr.* **1972**, 1–57.

Kristoffersen, F. N. & Bang, I. 1982. Cenozoic excl. Danian limestone. In: *Geology of the Danish Central Graben* (edited by Michelsen, O.). *Danmarks geol. Unders.* **B8**, 61–70.

Marrett, R. & Allmendinger, R. W. 1991. Estimates of strain due to brittle faulting: sampling of fault populations. *J. Struct. Geol.* **13**, 735–738.

Michelsen, O. (editor) 1982. *Geology of the Danish Central Graben. Danmarks geol. Unders.* **B8**.

Michelsen, O. & Andersen, C. 1981. Überblick über die regionale Geologie und Tektonik Dänemarks. *Z. angev. Geol.* **27**, 171–176.

Mikkelsen, L. P. 1988. Den strukturelle udvikling i Kridt og Tertiær af den nordvestlige del af dansk sektor, Nordsøen. Unpublished Masters, Aarhus University, Denmark.

Mogensen, T. E. 1988. Permo-Jurassisk strukturel udvikling af Central Truget i grænseområdet mellem Danmark og Norge. Unpublished Masters thesis, Aarhus University, Denmark.

Nicolas, A. & Poirier, J. P. 1976. *Crystalline Plasticity and Solid State Flow in Metamorphic Rocks*. John Wiley & Sons, London.

Nielsen, L. H. & Japsen, P. 1991. Deep wells in Denmark 1935–1990. *Danmarks geol. Unders.* **A31**.

Nielsen, O. B., Sørensen, S., Thiede, J. & Skarbø, O. 1986. Cenozoic Differential Subsidence of North Sea. *Bull. Am. Ass. Petrol. Geol.* **70**, 276–298.

Price, N. J. 1966. *Fault and Joint Development in Brittle and Semi-brittle Rock*. Pergamon Press, London.

Ramberg, H. 1981. *Gravity, Deformation and the Earth's Crust*. Academic Press, London.

Ramsay, J. G. 1967. *Folding and Fracturing of Rocks*. McGraw-Hill, New York.

Rundberg, Y. 1989. Tertiary sedimentary history and basin evolution of the Norwegian North Sea between 60°–62°N—An integrated approach. Unpublished thesis at NTH, Norway.

Schack Pedersen, S. A. 1987. Comparative studies of gravity tectonics in Quaternary sediments and sedimentary rocks related to foldbelts. In: *Deformation of Sediments and Sedimentary Rocks* (edited by Jones, M. E. & Preston, R. M. F.). *Spec. Publs geol. Soc. Lond.* **29**, 165–180.

Scholz, C. H. 1990. *The Mechanics of Earthquakes and Faulting*. Cambridge University Press, Cambridge.

Suppe, J. 1985. *Principles of Structural Geology*. Prentice-Hall, Englewood Cliffs, New Jersey.

Vejbæk, O. V. 1986. Seismic Stratigraphy and tectonic evolution of the Lower Cretaceous in the Danish Central Trough. *Danmarks geol. Unders.* **A11**.

Vejbæk, O. V. & Andersen, C. 1987. Cretaceous–Early Tertiary inversion tectonism in the Danish Central Trough. *Tectonophysics* **137**, 221–238.

Walsh, J. J. & Watterson, J. 1988. Analysis of the relationship between displacements and dimensions of faults. *J. Struct. Geol.* **10**, 239–247.

Walsh, J. J., Watterson, J. & Yielding, G. 1991. The importance of small-scale faulting in regional extension. *Nature* **351**, 391–393.

Winker, C. D. 1982. Cenozoic shelf margins, northwestern Gulf of Mexico. *Trans. Gulf Coast Ass. geol. Soc.* **32**, 427–448.

APPENDIX 1

The mathematics for calculating the strata parallel elongation due to a bending model is presented. The geometric relationships are shown in Fig. A1.

The length of the neutral surface segment bounded by the two radii (Fig. A1) is the initial length l_0 of the deformed segment.

The length of a layer L in the deformed state is l_1 and from Fig. A1

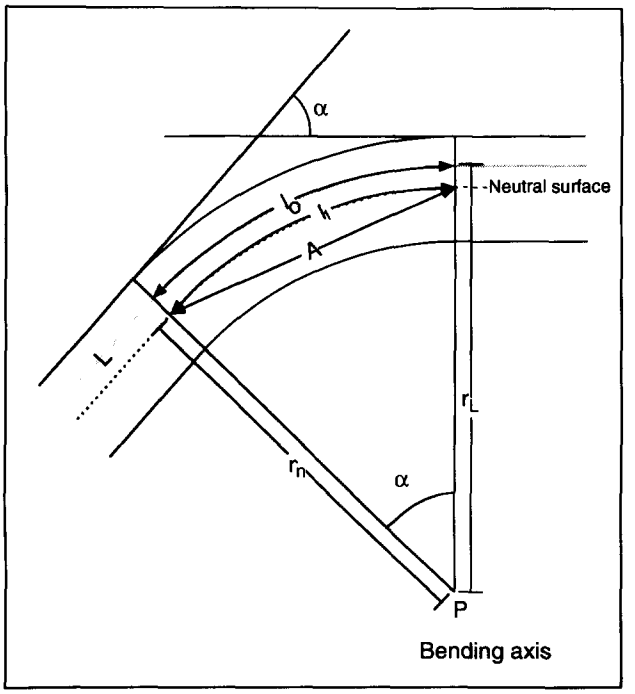

Fig. A1. Geometric relations of the bending model. L is the layer of interest, A is the chord between two radii intersecting the neutral surface, and α is the bending angle.

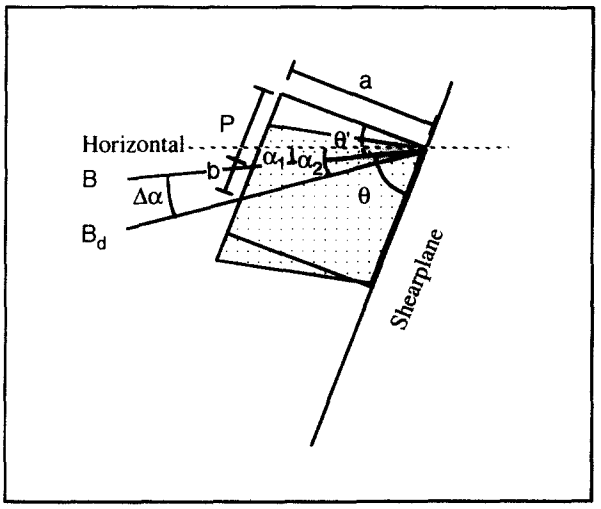

Fig. A2. The geometry of the simple shear model. All the symbols are referred to in the text. The initial state is represented by a square box with a side parallel to the shear plane, and the deformed state is the distorted square. $\Delta\alpha$ is the angle between a layer before (B) and after shearing (B_d). The elongation of the layer depends on the amount of simple shear strain (γ) and on the initial orientation with respect to the shear plane.

$$l_0 = r_n \cdot \frac{\alpha}{360} \cdot 2\pi = r_n \cdot \alpha \cdot \frac{\pi}{180} \tag{A1}$$

$$l_1 = r_L \cdot \frac{\alpha}{360} \cdot 2\pi = (r_n - \Delta r) \cdot \alpha \cdot \frac{\pi}{180} \tag{A2}$$

$$\Delta r = r_L - r_n, \tag{A3}$$

where r_n is the radius to the neutral layer and r_L is the radius to the layer L.

The elongation of layer L initially parallel to the neutral surface is:

$$\varepsilon = \frac{l_1}{l_0} - 1 = \frac{r_n + \Delta r}{r_n} - 1 = \frac{\Delta r}{r_n}. \tag{A4}$$

r_n can be expressed in terms of the chord A and the bending angle α

$$\sin\left(\frac{\alpha}{2}\right) = \frac{A}{2r_n} \tag{A5}$$

$$r_n = \frac{A}{2 \cdot \sin\left(\frac{\alpha}{2}\right)} \tag{A6}$$

and substituting into (A4)

$$\varepsilon_L = \frac{\Delta r \cdot 2 \cdot \sin\left(\frac{\alpha}{2}\right)}{A} \tag{A7}$$

which gives the elongation of the layer L.

Whether the elongation is positive or negative depends on the sign of Δr and equation (A3) emphasizes that the location of the neutral surface is important.

Equation (A7) is used to calculate the theoretical strain distribution used in the discussion of the deformation model.

APPENDIX 2

The mathematics for calculating the elongation generated by simple shear in a direction inclined to the shear plane is presented. The following relationships are based on the geometries shown in Fig. A2.

α_1 is the true dip of the undeformed strata, α_2 is the true dip of the deformed strata and

$$\Delta\alpha = \alpha_2 - \alpha_1. \tag{A8}$$

θ is the angle between the undeformed strata and the shear plane and from the geometric relationships in Fig. A2 we get the following relations between the distances P, a, b and the angle θ

$$\theta' = 90 - \theta \tag{A9}$$

$$\frac{P}{a} = \tan(\theta') \tag{A10}$$

$$\frac{b + P}{a} = \tan(\Delta\alpha + \theta'). \tag{A11}$$

The simple shear strain from a displacement b across a distance of a is (Fig. A2)

$$\gamma = \frac{b}{a}. \tag{A12}$$

Combining equations (A10)–(A12) gives

$$\gamma = \tan(\Delta\alpha + \theta') - \tan(\theta') \tag{A13}$$

which expresses the shear strain by the known angles $\Delta\alpha$ and θ'.

The initial length of a bed (B) inclined to the shear plane is

$$l_0 = \frac{a}{\cos(\theta')} \tag{A14}$$

and the length of the deformed bed (B_d, Fig. A2) is

$$l = \frac{a}{\cos(\theta' + \Delta\alpha)} \tag{A15}$$

which gives the strata parallel elongation

$$\varepsilon = \frac{l}{l_0} - 1 = \frac{\cos(\theta')}{\cos(\theta' + \Delta\alpha)} - 1. \tag{A16}$$

This simple relation shows that the amount of strata-parallel elongation is controlled by the same parameters as the shear strain. Therefore the strata-parallel elongation is constant parallel to the shear plane and may vary only normal to the shear plane. The sign of the strata-parallel elongation is constant due to the initial angular relationship. Assuming that the angular relationships prevail the sign may change only if the direction of movement on the shear plane is reversed.

APPENDIX 3

The mathematics for the stress–strain analysis of the simple bending model location A and location B in Fig. 14 is given here. Assuming that the bending at location A in Fig. 14 is comparable to the bending at location B (i.e. the curvature is the same, and the neutral surface is located at the top of the stratum) the elongation at B (ε^B) is related to the elongation at A (ε^A) by the equation

$$\varepsilon^A = -\varepsilon^B. \tag{A17}$$

The bending is a plane strain and the stratum parallel stress generated during bending

$$\sigma_b = E \cdot \varepsilon, \tag{A18}$$

depends thus on the amount of strata parallel stretching (ε) and Young's modulus (E) for the material (Price 1966, p. 149). This means that the bending causes a decrease in compressive strata-parallel stress at location A and an increase in strata-parallel compressive stress at location B since there is extension and compression at A and B, respectively, i.e.

$$=\sigma_b^B = \sigma_b^A < 0 \text{ and } |\sigma_b^B| = |\sigma_b^A| = \sigma_b. \tag{A19}$$

In the initial situation with no bending, the horizontal stress (σ_h) acting is proportional to the lithostatic pressure (σ_{lit}),

$$\sigma_h = k \cdot \sigma_{lit} = k \cdot D \cdot \mathbf{g} \cdot \rho, \tag{A20}$$

where D is the burial depth, ρ the density of the sediment, $\mathbf{g}$ the acceleration due to gravity and k is a positive factor less than 1 (Jaeger & Cook 1969, pp. 368–369) in some cases equals $\nu/(1-\nu)$ where ν is Poisson's ratio. Poisson's ratio has a value of 0.25–0.3 for most materials (Hobbs *et al.* 1976, p. 11, Nicolas & Poirier 1976, p. 84, Suppe 1985, p. 183). The resulting stratum parallel compressive stress

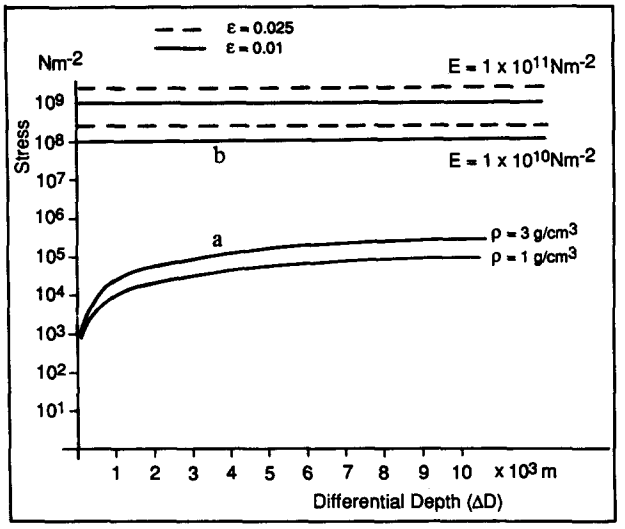

Fig. A3. Graph showing the variations in lithostatic pressure with depth for two sediment densities (curves at a). The curves at (b) show how the differential stress generated due to bending (σ_b) varies with Young's modulus (E) (Birch 1966) and the elongation due to bending according to equation (5) (Price 1966). If the depth axis is considered to be a differential depth axis the curves at (a) illustrate the difference in lithostatic pressure between location A and B in Fig. 14. The relations between the two sets of curves clearly illustrate that $\Delta D \cdot \mathbf{g} \cdot \rho \ll \sigma_b$ and that $\sigma_b > (1 - k) \cdot \sigma_{lit}^B$ even for minor bending (small values of ε).

(σ_{SP}^A) at location A due to bending is thus derived from a reduction of the horizontal stress (σ_h^A) by the generated 'bending stress' (σ_b)

$$\sigma_{SP}^A = \sigma_h^A - \sigma_b. \quad \text{(A21)}$$

The resulting stratum parallel compressive stress (σ_{SP}^B) at location B is

$$\sigma_{SP}^B = \sigma_h^B - \sigma_b. \quad \text{(A22)}$$

The stress perpendicular to the bending induced stress is sub-vertical and assumed equal to the lithostatic pressure (σ_{lit}).

Since the direction of the stratum parallel stress parallels a principal direction of stress and the principal stresses at location A are

$$\sigma_1^A = \sigma_{lit}^A \quad \text{(A23a)}$$

$$\sigma_3^A = \sigma_{SP}^A \quad \text{(A23b)}$$

since $\sigma_{SP}^A < \sigma_{lit}^A$. At location B we have

$$\sigma_1^B = \sigma_{SP}^B \quad \text{(A24a)}$$

$$\sigma_3^B = \sigma_{lit}^B \quad \text{(A24b)}$$

if $\sigma_b > (1 - k) \cdot \sigma_{lit}^B$ (equations A20 and A22) which is the case even at very small amounts of bending (Fig. A3).

When drawing the relative location of the Mohr stress circles for location A and B it is necessary to know the differential stress at each location and the relative size of σ_3^A and σ_3^B.

The differential stress at A from equations (A20), (A21) and (A23) is

$$\sigma_1^A - \sigma_3^A = \sigma_{lit}^A - \sigma_{SP}^A = \sigma_{lit}^A - k \cdot \sigma_{lit}^A + \sigma_b = (1 - k) \cdot \sigma_{lit}^A + \sigma_b \quad \text{(A25)}$$

and the differential stress at B from to equations (A20), (A22) and (A24) is

$$\sigma_1^B - \sigma_3^B = \sigma_{SP}^B - \sigma_{lit}^B = k \cdot \sigma_{lit}^B + \sigma_b - \sigma_{lit}^B - = (k - 1) \cdot \sigma_{lit}^B + \sigma_b. \quad \text{(A26)}$$

Since $0 < k < 1$ we have

$$\sigma_1^A - \sigma_3^A > \sigma_b > \sigma_1^B - \sigma_3^B \quad \text{(A27)}$$

which means that the differential stress at B is smaller than at A.

The relations between the lithostatic pressures at A and B is

$$\sigma_{lit}^A = \sigma_{lit}^B + \Delta D \cdot \mathbf{g} \cdot \rho, \quad \text{(A28)}$$

where ΔD is the difference in burial depth of location A and B (Fig. 14). Inserting the relations to the principal stresses (equations A23 and A24) in equations (A20), (A21) and (A28) gives

$$\sigma_1^A = \sigma_3^B + \Delta D \cdot \mathbf{g} \cdot \rho \quad \text{(A29)}$$

$$\sigma_3^A = k \cdot \sigma_1^A - \sigma_b \quad \text{(A30)}$$

$$\sigma_3^A = k \cdot (\sigma_3^B + \Delta D \cdot \mathbf{g} \cdot \rho) - \sigma_b, \quad \text{(A31)}$$

where equation (A31) expresses the relation between the least compressive stress at location A and location B in Fig. 14.

Assuming that $\sigma_3^A < \sigma_3^B$ we have

$$\sigma_3^B > k \cdot (\sigma_3^B + \Delta D \cdot \mathbf{g} \cdot \rho - \sigma_b. \quad \text{(A32)}$$

Since $(\sigma_3^B + \Delta D \cdot \mathbf{g} \cdot \rho) > k \cdot (\sigma_3^B + \Delta D \cdot \mathbf{g} \cdot \rho)$ we have

$$\sigma_3^B > \sigma_3^B + \Delta D \cdot \mathbf{g} \cdot \rho - \sigma_b \quad \text{(A33)}$$

which means that $\sigma_3^A < \sigma_3^B$ for

$$\Delta D \cdot \mathbf{g} \cdot \rho < \sigma_b. \quad \text{(A34)}$$

Figure A3 shows that the bending stress is larger than the difference in lithostatic pressure between A and B, even for extreme values of Young's modulus and elongation. The Mohr circle for the stresses at location A is therefore located to the left of the Mohr circle for the stresses at location B, and the radius of the circle is larger in A than in B (Fig. 15).